Wenyan Li[1]
Giacomo Vacca[2]
Maryann Castillo[3]
Kevin D. Houston[3]
Jessica P. Houston[1]

[1]Department of Chemical Engineering, College of Engineering, New Mexico State University, Las Cruces, NM, USA
[2]Kinetic River Corp., San Jose, CA, USA
[3]Department of Chemistry and Biochemistry, College of Arts and Sciences, New Mexico State University, Las Cruces, NM, USA

Received December 7, 2013
Revised March 14, 2014
Accepted March 18, 2014

Research Article

Fluorescence lifetime excitation cytometry by kinetic dithering

Flow cytometers are powerful high-throughput devices that capture spectroscopic information from individual particles or cells. These instruments provide a means of multiparametric analyses for various cellular biomarkers or labeled organelles and cellular proteins. However, the spectral overlap of fluorophores limits the number of fluorophores that can be used simultaneously during experimentation. Time-resolved parameters enable the quantification of fluorescence decay kinetics, thus circumventing common issues associated with intensity-based measurements. This contribution introduces fluorescence lifetime excitation cytometry by kinetic dithering (FLECKD) as a method to capture multiple fluorescence lifetimes using a hybrid time-domain approach. The FLECKD approach excites fluorophores by delivering short pulses of light to cells or particles by rapid dithering and facilitates measurement of complex fluorescence decay kinetics by flow cytometry. Our simulations demonstrated a resolvable fluorescence lifetime value as low as 1.8 ns ($\pm$0.3 ns) with less than 20% absolute error. Using the FLECKD instrument, we measured the shortest average fluorescence lifetime value of 2.4 ns and found the system measurement error to be $\pm$0.3 ns (SEM), from hundreds of monodisperse and chemically stable fluorescent microspheres. Additionally, we demonstrate the ability to detect two distinct excited state lifetimes from fluorophores in single cells using FLECKD. This approach presents a new ability to resolve multiple fluorescence lifetimes while retaining the fluidic throughput of a cytometry system. The ability to discriminate more than one average fluorescence lifetime expands the current capabilities of high-throughput and intensity-based cytometry assays as the need to tag one single cell with multiple fluorophores is now widespread.

Keywords:
Bioanalytical / Flow cytometry / Fluorescence decay / Fluorescence lifetime / Time-resolved
DOI 10.1002/elps.201300618

1 Introduction

For decades, fluorescence-based flow cytometry measurements have enhanced cell biology research and enabled many advances in disease diagnosis for the biomedical community [1]. Flow cytometers offer a unique capability for single-cell analysis and the separation of large populations of cells at high throughput. Flow cytometers, in general, drive cells through the path of a laser beam at laminar flow rates to capture light scatter and fluorescence signatures emitted from individual cells [2]. This method, combined with a controlled binding of organic fluorophores to different cellular organelles, proteins, nucleic acids, or other cellular constituents [3], enables powerful multi-parametric analysis of large cell populations (i.e. 1×10^6) in a matter of minutes. A rise in the synthesis of new organic fluorophores and in the development of a variety of fluorescent proteins has, in parallel with improvements in flow cytometry instrumentation, allowed new capabilities where as many as nine or more intracellular features can be detected from thousands of cells in a few seconds [3]. Although an increase in the number of photodetector color channels on a flow cytometer enhances the instrument, difficulties remain with the ability to evaluate spectral data when the emission of intrinsic and extrinsic fluorophores significantly overlaps. In flow cytometry, fluorescence compensation algorithms are used to correct datasets with spectral overlap issues yet these processing tools remain inadequate for severe spectral overlap scenarios, and are complicated for cytometrists in clinical settings.

To address the issue of spectral overlap, the fluorescence lifetime has been incorporated as an additional detection parameter. Although this capability is not a common feature of commercially available instruments, it has increased the utility of flow cytometry by providing intensity-independent measurements [4–8]. The fluorescence lifetime is the average

Correspondence: Dr. Jessica P. Houston, Department of Chemical Engineering, College of Engineering, New Mexico State University, Las Cruces, NM 88003-001, USA
E-mail: jph@nmsu.edu
Fax: +1-575-646-7706

Abbreviations: CHO, Chinese hamster ovary; **EB**, ethidium bromide; **FLECKD**, fluorescence lifetime excitation cytometry by kinetic dithering; **FWHM**, full-widths at half maximum; **TCSPC**, time-correlated single-photon counting

time a fluorophore spends in its excited state prior to decaying back to the ground state; this parameter is a unique feature of a given fluorophore and can be impacted by the fluorophore's microenvironment or other molecular quenchers [9]. Some groups, including our own, have demonstrated the use of average fluorescence lifetime measurements by flow cytometry to alleviate issues associated with spectral overlap [10], to eliminate autofluorescence interference [11], to quantitatively measure Förster resonance energy transfer [12], to determine intracellular environmental changes [13], and to track protein localization within a cell [14]. The standard method for measuring the fluorescence lifetime in a flow cytometer has mainly involved frequency-domain systems [4, 6, 7]. With frequency-domain techniques, the laser excitation source is modulated at a radio frequency, and the fluorescence emission is measured to capture the phase-shift of fluorescence relative to excitation. The phase shift is due to the inherent fluorescence decay kinetics of the excitable fluorophore. According to Eq. (1), the phase shift θ is proportional to the fluorescence lifetime, τ, and inversely proportional to the excitation modulation frequency f ($\omega = 2\pi f$) when single-exponential fluorescence decay is assumed. However the phase-sensitive (frequency-domain) fluorescence lifetime approach is unable to resolve multi-exponential fluorescence decays. Detection of multiple lifetimes by frequency-based methods requires multi-frequency systems, typically implemented in the context of static fluorimetry or fluorescence lifetime imaging microscopy. Owing to the transient nature of the light–cell interaction in a flow cytometer, the amount of time (~2–5 μs) during which the fluorescence lifetime can be measured is too short to allow multi-frequency measurements on a cell-by-cell basis:

$$\tau = \frac{\tan\theta}{\omega}. \quad (1)$$

In this work, we present a paradigm shift in the instrumentation architecture of a flow cytometer capable of measuring fluorescence lifetime. In lieu of standard frequency-domain techniques, a new type of time-resolved instrument was conceived for the purpose of expanding the ability to measure multiple fluorescence decays from single, transient events. The new approach takes advantage of the time delay between the fluorescence signal and the side scatter signal, similar to the phase delay between emission and excitation in multi-frequency systems. As a cell interacts with the laser beam, a prototypical Gaussian peak results from the interaction between the cell and the interrogating light beam, which normally has a Gaussian profile in the direction of flow (see Fig. 1). When shifts in the fluorescence lifetime between the scattering and fluorescence signals are to be detected on the order of nanoseconds, the width of the signal pulses becomes a limiting factor. Therefore reducing the width of the Gaussian interaction peak may improve the measurement of fluorescence-lifetime-induced time delays and achieve the resolution necessary for accurate fluorescence lifetime measurements (Cao R. et al., submitted).

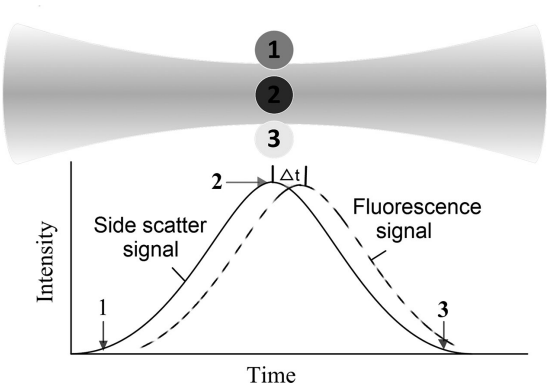

Figure 1. Illustration of a laser beam waist with a Gaussian intensity profile interacting with a cell (circular shape). As a cell enters the beam at 1, is fully illuminated at 2, and leaves the beam at 3, fluorescence emission (and corresponding light scatter) increases from 0 to its peak value and then decreases to 0 (bottom). The finite fluorescence lifetime causes a time delay $\Delta\tau$ of the fluorescence signal.

In this paper, we describe a new method to measure multiple fluorescence lifetimes without frequency-domain laser modulation; our approach is based on reducing the width of the correlated scatter and fluorescence pulses. We refer to the method as fluorescence lifetime excitation cytometry by kinetic dithering (FLECKD). The FLECKD instrument concept is rooted in time-domain measurement analysis. In the time-domain a short excitation pulse, typically represented as a delta function, is delivered to a static sample (i.e. a cell or group of cells), and the subsequent fluorescence emission is observed for a finite amount of time. A fluorescence detector is gated to observe this fluorescence decay. This method is known as time-correlated single-photon counting (TCSPC) [15, 16]. Detecting the full fluorescence decay profile results in datasets that can be regressed for lifetime values regardless of the type of exponential decay. Early demonstrations include TCSPC-based fluorimeters and microscopes [17–26], and modern fluorescence lifetime imaging microscopy systems contain rapid data acquisition and powerful data/image processing algorithms [27–32]. Likewise, the FLECKD system permits detection of full fluorescence decay profiles yet does not involve imaging a stationary cell, group of cells, or tissue section. With the FLECKD system, moving cells are interrogated rapidly which makes this fluorescence lifetime measurement ideal for cell sorting assays involving fluorescence protein expression, metabolic mapping by autofluorescence lifetime changes, and fluorescence multiplexing [33–39].

In the following we detail the development of FLECKD and demonstrate how it can be used to extract more than one fluorescence lifetime while preserving standard cytometric throughput. The instrumentation is described as are modeling results and experimental results that demonstrate the performance of the system under four conditions: (i) single-exponential fluorescence decay samples; (ii) multi-exponential fluorescence decay samples; (iii) fluorescence lifetime changes induced by quenchers; and (iv) fluorescence lifetimes exhibited by fluorescent proteins in living cells.

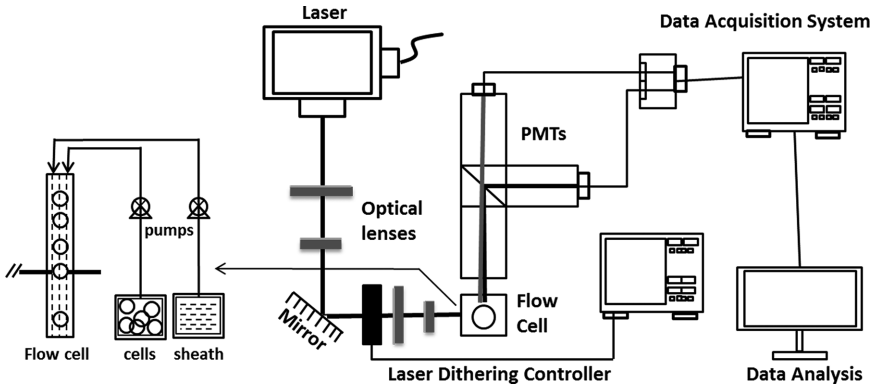

Figure 2. Schematic of the fluorescence lifetime excitation cytometry by kinetic dithering (FLECKD) system.

2 Materials and methods

2.1 Instrumentation

In contrast to the standard laser transit times (typ. 2–10 μs) of commercial cytometry systems, the FLECKD instrument produces interaction times smaller by at least two orders of magnitude (~25 ns). Rapid excitation of fluorescently labeled cells is achieved by moving the laser across the flowing particle/cell in a lateral direction (i.e. laser moves horizontally while cell moves vertically). The FLECKD system (custom model Gen-1 Danube™, Kinetic River, San Jose, CA, USA) was designed to include a rapidly dithering module onto a standard cytometric system configuration. The instrumentation includes: (i) an optical excitation module, (ii) fluidic components, (iii) an optical collection module, and (iv) a data acquisition system. Data analysis is performed off-line using custom-developed algorithms (Fig. 2 and described later). Briefly, cells and microspheres are driven at laminar velocities for single-file alignment through a 'flow chamber.' A syringe pump controls volumetric flow rates of 20 μL/min for the core (cells/microspheres in suspension) flow and 2000 μL/min for the sheath (i.e. surrounding water) flow. The fluidic specifications are adjustable for increased throughput. During flow a 300-mW, 532-nm laser (#532L-300-C0L-PP, Oxxius, Lannion, France) generates a Gaussian-profiled beam, which is propagated through several beam-shaping elements (optics, lenses) and is delivered to the fluidic chamber. In order to create the rapid laser–cell interaction times, the continuous wave laser beam is passed through an acousto-optic deflector (#AODF 4545–121, Crystal Technology, Palo Alto, CA, USA), aligned, and optimized for first-order diffraction ($2\theta = 1.82°$). The deflector is driven by a radio-frequency (RF) function generator (sawtooth, 2 MHz frequency, 1 Vpp amplitude, 1.145 V offset) coupled with a linear voltage-controlled oscillator (VCO) and RF amplifier (1250FM-1 2.0W, Crystal Technology). The sawtooth causes the VCO to generate a chirped RF wave and therefore change the diffraction angle in the AODF (±0.25°), resulting in the translation of the beam across the core stream at the frequency of the saw tooth waveform. The falling edge of the sawtooth is designed to be short in order to accomplish a minimum laser beam 'flyback' time. The laser beam can be characterized as "dithering" by its rapid change in position across the core stream. When cells and microspheres flow through the chamber, they are excited by the beam as it transit across the core stream, resulting in a "pulse" of light ~25 ns wide. Repeated dithering results in multiple excitation pulses (~100) across each moving cell. Three detectors are placed around the chamber for measurement of the resulting optical signals. The extinction signal from the forward-propagating beam exiting the flow chamber is collected by a photodiode, which is helpful for calibration. Additionally, side-scattered light (532-nm band pass filter; 90 degrees to laser excitation) and fluorescence emission (550-nm long pass filter; 90 degrees to laser) are collected with photomultiplier tubes (PMT #R636–10, Hamamatsu Photonics K.K., Hamamatsu City, Japan). The current signals from each photodetector are converted to voltage pulses, amplified (#DC-100, Advanced Research Instruments, Golden, CO, USA) and digitized with an oscilloscope (#TDS 2024B, Tektronix, Beaverton, OR, USA; 200MHz bandwidth, 2GS/s sampling rate, 2.5K record length). All datasets are analyzed in MATLAB (The Mathworks®, Natick, MA, USA). Each signal-processing algorithm is developed in-house with the help of the FluorFit1.2 toolbox (www.fluortools.com).

2.2 Theory

FLECKD theory is based on the idea that the changes in the fluorescence decay kinetics of a given fluorophore will cause a shift in the average time at which fluorescence photons are detected relative to the average time at which scattered photons are detected. This principle is illustrated in Fig. 1 (Cao R. et al., submitted). As a laser beam is scanned across a cell, the fluorescence lifetime can be measured by comparing the time delay between the photons recovered from the fluorescence signal and those instantaneously and elastically scattered in the side direction. Moreover, by shortening the light–cell interaction time, the FLECKD system makes the decay behavior directly observable (i.e. a decay-like shape in the emission signal relative to the scatter signal is recorded).

To compute complex relaxation kinetics of excited fluorophores, additional processing is performed on the full

fluorescence and scattering waveforms. A mathematical description of this process involves convolution because the observed fluorescence decay is a function of the instrumental response. Specifically, the captured side-scattered signals, or waveforms, are a convolution of the laser intensity profile, the volume of the cell, and electronic system noise. The mathematical framework involves parameters such as the core stream flow velocity, the diameter of fluorescence microspheres and mammalian cells (7–15 μm, assumed spherical), and the laser beam waist profile at the core stream (Gaussian, (0,0) mode, 2 $w_0 \sim 20$ μm). Likewise, the fluorescence waveforms are a convolution of the same factors; however the fluorescence decay might take the shape of any one of a family of multi-exponential curves, depending on the fluorescent molecules present and factors that affect their lifetime. Thus the fluorescence waveform shape changes, and mathematically it is represented by a convolution of the side-scattered waveforms and exponential decay functions.

Early mathematical models [40] have described the convolution of a Gaussian function and exponential curve as the "ex-Gaussian" curve. Equation (2) represents the ex-Gaussian function, with t representing the average fluorescence lifetime:

$$f(x|\mu,\sigma,\tau) = \frac{1}{2} exp\left[\frac{\mu}{\tau} + \frac{\sigma^2}{2\tau^2} - \frac{x}{\tau}\right] \varnothing\left[\frac{x-\mu-\frac{\sigma^2}{\tau}}{\sigma}\right] \quad (2)$$

However, single exponential decays described by the ex-Gaussian function of Eq. (2) only assume a single fluorescence lifetime. In order to properly represent multi-exponential fluorescence decays, a deconvolution approach can be employed. Because added system noise makes straightforward deconvolution impossible, an iterative reconvolution of the theoretical model with the measured instrument response (scatter light signal) is necessary to find the optimum fit to the fluorescence signal. Fourier convolution theorem is used in the reconvolution process, and the minimum least-squares error is found by changing the theoretical decay model to best fit the experiment data. The fluorescence lifetime value is calculated by comparing the model to the experimental data, and the model with a fluorescence lifetime that best fits the experimental data (i.e. smallest experiment-to-model mismatch, or minimum least squares error) is identified. A conclusion is then made with the identified model to best approximate the fluorescence lifetime.

The detailed process involves taking the convolution of a Gaussian function with an appropriate multi-exponential decay model, and then performing a deconvolution to resolve the various fluorescence lifetime contributions.

$$f * g(t) = \int_{x=0}^{t} f(x)g(t-x)dx \begin{cases} e.g.\ f(x) = ae^{\frac{(x-b)^2}{2c^2}} + d \\ e.g.\ g(x) = \sum_{i=1}^{n} a_i * \exp\left(-\frac{t}{\tau_i}\right) \end{cases} \quad (3)$$

This is described by Eq. (3), where $f^*\ g(t)$ is the convolution of two functions: the Gaussian function $f(x)$ and the decay function $g(x)$. With real or simulated data, a deconvolution will separate the instrument-response function $f(x)$, which is accurately approximated by side-scatter signals, from the observed fluorescence signals $f^*\ g(t)$, yielding the desired fluorescence decay curve, $g(t)$.

2.3 Simulations

Simulations to support the theory described above and demonstrate the significance of the shortened excitation times made possible by the FLECKD technique involved construction of canonical Gaussian excitation waveforms and ex-Gaussian fluorescence waveforms for a range of fluorescence lifetimes, combinations of fluorescence lifetimes, and instrument response function widths. Four sets of simulations were carried out: (S1) an ex-Gaussian curve with a 10-ns exponential decay compared with three Gaussian curves with different widths (full-widths at half maximum—FWHM—of 1.5 μs, 15 ns, and 15 ps); (S2) ex-Gaussian curves with a common 15-ns Gaussian width and 1-, 6-, 11-, 16-, 21-, 26-, and 31-ns exponential decays; (S3) ex-Gaussian curves with a common 15-ns Gaussian width and mixed lifetime decays of (i) 70% 2 ns and 30% 15 ns, (ii) 30% 2 ns and 70% 15 ns, (iii) 70% 8 ns and 30% 15 ns, and (iv) 70% 2 ns and 30% 22 ns; and (S4) two ex-Gaussian curves with a common 15-ns Gaussian width and mixed lifetime decays of 70% 2 ns and 30% 22 ns, and a single lifetime of 18.5 ns (the mean lifetime of 70% 2 ns and 30% 22 ns, calculated with Eq (4):

$$\tau_{mean} = \frac{\sum_{i=1}^{n} a_i * \tau_i^2}{\sum_{i=1}^{n} a_i * \tau_i}. \quad (4)$$

In addition to the S1–S4 simulations, other simulated data were generated to evaluate the fluorescence lifetime resolution. Simulations with fluorescence lifetime values of 0.5-, 0.7-, 1-, 1.3-, 1.4-, 1.5-, 1.6-, 1.7-, 1.8-, 1.9-, 2-, 2.1-, 2.2-, 2.5-, 3-, 4-, 5-, 6-, 7-, 8-, and 10-ns were tested. Convolution of the single-exponential decay and a real side-scatter signal was computed, and the convolution product was processed with noise (normal distribution, $n = 2500$, stdev $= 1$, $\mu = 0$). The random noise increased the noise floor by a factor of 0.03, and was determined by the amplitude ratio of the noise to the actual and normalized side scatter signal. Finally the simulations are compared as described previously to determine how closely the fit matches the simulated fluorescence lifetime (i.e. perfect fits result when no noise is added). Artificial noise was generated to mimic noise from optical measurements, electronics, and data acquisition and obtain a best approximation of the lifetime resolution.

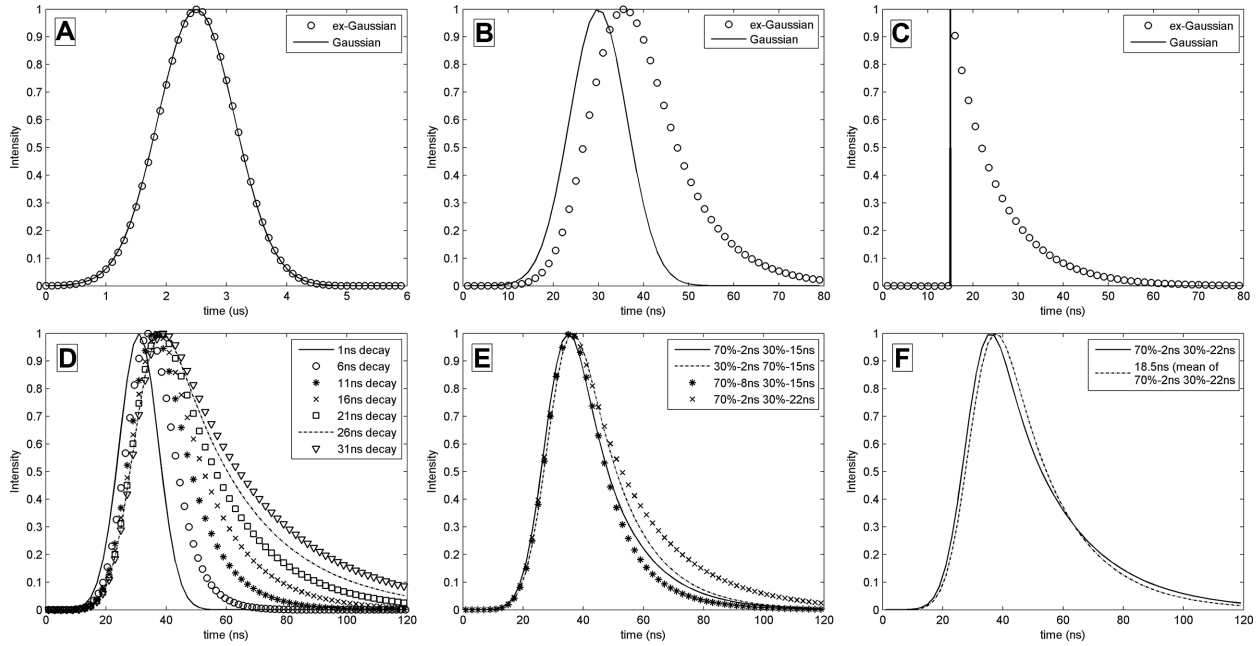

Figure 3. Sets of simulations performed to model side scatter and fluorescence waveforms. (A), (B), (C) Gaussian functions (—) representing side-scatter waveforms with 1.5 μs, 15 ns, and 15 ps FWHM, respectively. The ex-Gaussian curves (o) were obtained by convolving each Gaussian function with a 10-ns exponential decay. (D) Ex-Gaussian curves produced by a Gaussian function (15-ns FWHM) convolved with 1– (—), 6-(o), 11– (*), 16– ($_x$), 21– ($_\square$), 26– (—) and 31-ns ($\triangledown$) exponential decays. (E) Ex-Gaussian curves produced by a Gaussian function (15-ns FWHM) convolved with multi-exponential decays (A1 = 0.7, τ1 = 2 ns; A2 = 0.3, τ2 = 15 ns) (—), (A1 = 0.3, τ1 = 2 ns; A2 = 0.7, τ2 = 15 ns) (—), (A1 = 0.7, τ1 = 8 ns; A2 = 0.3, τ2 = 15 ns) (*), and (A1 = 0.7, τ1 = 2 ns; A2 = 0.3, τ2 = 22 ns) ($_x$), respectively. (F) Two ex-Gaussian curves obtained by a convolution of a Gaussian function (15-ns FWHM) with a double-exponential decay function (A1 = 0.7, τ1 = 2 ns; A2 = 0.3, τ2 = 22 ns) (—) and mean lifetime of 18.5 ns (70% 2 ns and 30% 22 ns) (—).

2.4 Experiments with fluorescent microspheres and cells

The fluorescent microspheres used for lifetime evaluation included: Flow-Check™ Fluorospheres (number 6605359, 10 μm, Beckman Coulter, Brea, CA, USA) and SPHERO™ Fluorescent Nile Red Particles (Cat. number FP-6056–2, 6 μm, Spherotech, Lake Forest, IL, USA).

Chinese hamster ovary cells (CHO-K1, American Type Culture Collection) were cultured in Dulbecco's medium (Life Technologies, Carlsbad, CA, USA) containing 10% fetal bovine serum in a cell culture incubator maintaining 37°C and 5% CO_2 atmosphere. For CHO-K1 experiments cells were labeled with ethidium bromide (EB) (Lot # A0250299, ACROS Organics, Geel, Belgium). EB intercalates into DNA and is a common cell-cycle fluorophore. Thus cells were collected in the exponential phase of growth using trypsin, counted, and re-suspended at a concentration of 10^6 cells/mL in PBS without calcium or magnesium. Cells were then fixed in 70% ethanol and stained with 3 μg/mL EB in PBS containing 20 μg/mL RNase A (number 1007885, Qiagen, Venlo, Limburg, Netherlands). These experiments were performed with and without addition of the known EB quenching agent, amsacrine (number A9809, Sigma Aldrich, St. Louis, MO, USA) [41]. In other CHO-K1 cultures transfection using the oChIEF-tdTomato in AAV2 vector containing plasmid (Tsien Laboratory, University of California San Diego, San Diego, CA, USA) was performed using lipofectamine reagent (Life Technologies) following the manufacturer's protocol. Cells were maintained for 1–3 days posttransfection. Cells were collected using trypsin and resuspended in PBS (10^6 cells/mL) prior to measurement.

3 Results and discussion

3.1 Simulation results

Plots in Fig. 3 are simulation results for the Gaussian and ex-Gaussian function sets (S1–S4) described previously. Figure 3A, B, and C is of three different excitation pulse widths using simulation set S1, emphasizing how the light–cell interaction time dramatically impacts the ability to observe fluorescence decay in an ex-Gaussian curve. Figure 3A shows that the ex-Gaussian curve (Fig. 3A, 'o') synthesized by the convolution of a 1.5-μs Gaussian curve with a 10-ns exponential decay is visually indistinguishable from the Gaussian curve itself (Fig. 3A, '—'). Therefore with added system noise, which is expected with real data, a 10-ns decay would be very difficult to deconvolve from a 1.5-μs pulse. Instruments performing TCSPC techniques typically use excitation pulses in the picosecond range; therefore compared to a 10-ns decay curve, a Gaussian excitation function with a 15-ps width resembles a "delta function" (Fig. 3C, '—'), making

the convolution decay curve stand out very clearly (Fig. 3C, 'o'). However, TCSPC is designed for thousands of repeated excitations of stationary samples, which are unsuitable for the high-throughput single-pass-measurement requirements of flow cytometry. Therefore results that mimic the FLECKD system are provided in Fig. 3B, which plots a 15-ns Gaussian excitation curve (Fig. 3B, '—') and the simulated emission, or ex-Gaussian plot, resulting from convolution with a 10-ns decay function (Fig. 3B, 'o'). The simulation results in Fig. 3A, B, and C illustrate the point that excitation pulse widths of typical flow cytometers are not sufficient to directly time-resolve fluorescence decays and conversely picosecond excitation widths, albeit optimum for high resolution, are too narrow for flow cytometry. Therefore excitation pulse widths that are on the same order of magnitude as the sought-after fluorescence lifetime decay values can be adequate to produce the required time resolution.

Also in Fig. 3 are simulation results (sets S2, S3, and S4) that illustrate the concept of extracting single- as well as double-exponential decays from ex-Gaussian curves. Figure 3D (corresponding to simulation set S2) is a plot of ex-Gaussian fluorescence waveforms with lifetimes of 1-, 6-, 11-, 16-, 21-, 26-, and 31-ns. As the decay lifetime increases, the ex-Gaussian curve shifts more to the right, resulting in a longer "tail." In the case of mixed fluorescence lifetime ex-Gaussian waveforms (Fig. 3E, simulation set S3), high-intensity short lifetimes tend to lower the tail, while high-intensity long lifetimes raise the tail. Finally, Fig. 3F (simulation set S4) displays the results for ex-Gaussian curves with mixed lifetime values matching the EB decay times. We simulated different contributions of EB lifetimes to show their effect on the shape of the convolution curve.

Table 1 shows that at 1.8 ns (+/−0.3 ns), the difference between the simulated and fitted fluorescence lifetime was less than 20%. This value can be considered as the minimum measurable fluorescence lifetime reproduced with the best accuracy. This value however is a function of the width of the excitation pulse and the electrical noise. If no noise is added, the calculated fluorescence lifetime will be identical to the original simulation input lifetime.

Table 1. Summary of the simulation results for a variety of fluorescence waveforms with different fluorescence lifetimes

True lifetime (ns)	Calculated lifetime (ns)	Error (%)	True lifetime (ns)	Calculated lifetime (ns)	Error (%)
0.5	0.17	66	2.1	1.8	13
0.7	0.34	51	2.2	1.8	17
1	0.62	37	2.5	2.3	8
1.3	0.93	29	3	2.8	6
1.4	0.93	34	4	3.7	8
1.5	1	32	5	4.7	7
1.6	1.2	25	6	5.7	5
1.7	1.4	18	7	6.8	2
1.8	1.4	22	8	7.6	5
1.9	1.6	16	10	9.7	3
2	1.6	20			

The 'true lifetime' column provides simulated data using Eq. (3) by a convolution of a Gaussian function with random noise and single-exponential decay functions. The fit of each simulated fluorescence waveform was determined by finding the optimum lifetime (noted as 'calculated lifetime') at minimum fitting error. The calculated lifetimes are listed in the second column. The absolute error percentages between the true lifetimes and the calculated lifetimes are listed in the third column.

3.2 Single exponential decays

Figure 4 presents light scatter and fluorescence emission waveforms collected by the FLECKD system. Two types of fluorescent microsphere samples were measured: FlowCheck™ Fluorospheres and SPHERO™ Fluorescent Nile Red Particles. The waveforms represent the digitized signals of a single light–cell interaction event for each type of microsphere. Full widths at half maximum of the excitation pulses were obtained through fitting a Gaussian function to the side-scatter waveform. The scattered intensity profiles can be represented by a Gaussian function because the duration of the light–cell interaction dominates over detector bandwidth and particle size. The FWHM was calculated ($FWHM = 2\sqrt{2ln2}\sigma, \sigma = std\ dev$) and ranged from 25 to 30 ns with a SD of 1.85 ns (normalized data, mean $\chi^2 = 1.82$). The scattering process is nearly instantaneous making the side-scattered pulse an adequate representation of the instrument response function. On the other hand, the fluorescence intensity waveforms depend heavily on the fluorescence relaxation function as well as the Gaussian-like profile, resulting in the fluorescence signals shown in Fig. 4 (i.e. a longer tail than the scattering waveforms). With the microsphere measurements approximately 1000 events were collected, averaged, and analyzed with a single-exponential fluorescence decay function. When convolution and deconvolution were performed, the resulting function was found to fit each sample with an average ${\chi^2}_{red}$ residual of 0.0039 and a S.E.M. of +/− 0.3 ns. The fluorescence microspheres are manufactured to be physically monodisperse and chemically identical hence the S.E.M. represents the system measurement errors. The fluorescence lifetimes measured for the SPHERO™ Fluorescent Nile Red Particles and FlowCheck™ Fluorospheres were 4.0 ns (normalized-data ${\chi^2}_{red} = 0.0012$) and 8.0 ns (normalized-data ${\chi^2}_{red} = 0.0038$), respectively (Fig. 4A and B). These values are corroborated by previously measured values [4, 42].

3.3 Double exponential decays

EB-stained DNA in CHO-K1 cells was measured and analyzed with both single- and double-exponential decay models. Our results show that the fluorescence decay of EB fits the single and double exponential decay models with normalized

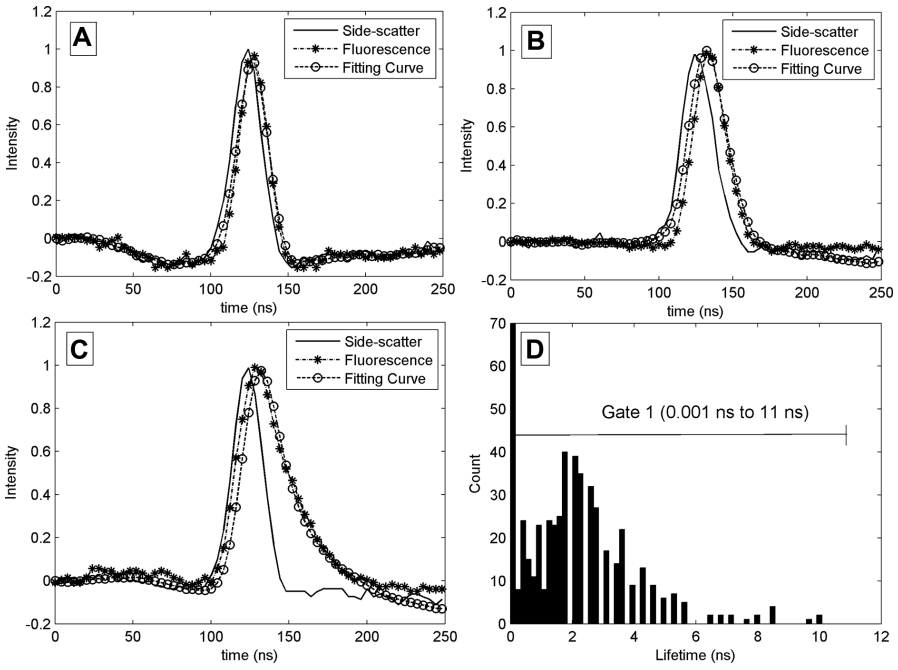

Figure 4. Experimental data waveforms (side scatter, —) (Fluorescence, —*—) and fitting curves (Fitting, —o—) were obtained by measuring fluorescence particles and EB-stained CHO K1 cells with the FLECKD system. (A) Nile Red particles, (B) Flow-Check Fluorospheres™, and (C) DNA-bound EB. Panel (D) is a distribution of fluorescence lifetime values obtained from cells expressing tdTomato.

χ^2_{red} values of 0.0056 and 0.0038, respectively. EB is known to have two dominant fluorescence lifetimes—longer when intercalated into cellular DNA, and shorter when not [43]. The long-lifetime component had a dramatic influence on the shape of the fluorescence waveform. The measured width of the fluorescence waveform was roughly twice that of the side-scattered waveform; additionally the tail of the EB signal was considerably extended in comparison to the excitation pulse. The two lifetime components extracted from the fit to the measured data were 25.5 ns and 4.9 ns (Fig. 4C). The inferred fluorescence lifetimes confirm measured EB lifetime values of prior work [44].

3.4 Fluorescence quenching

EB-stained CHO-K1 cells were treated with varying concentrations of the fluorescence quencher amsacrine. Others have proposed that DNA-bound amsacrine is an electron donor, transferring electrons to DNA-bound EB when both amsacrine and EB are in an excited state and within a certain distance of each other [41,45]. Therefore amsacrine was added to different groups of cells at 18.6 μM, 27.9 μM, and 37.2 μM concentrations to test for lifetime changes in EB. First the fluorescence intensity was evaluated for ~100 cells in each group, and the mean intensity was found to be reduced by 2%, 19%, and 24% for the 18.6 μM, 27.9 μM, and 37.2 μM concentrations, respectively. Table 2 lists all the measured fluorescence lifetime and intensity changes. When the DNA-bound EB was quenched with differing concentrations of amsacrine and its fluorescence intensity decreased 2%, 19%, and 24%, the mean fluorescence lifetime was shortened, from its original value of $\tau_1 = 15.9$ ns and $\tau_2 = 0.9$ ns (mean $\chi^2_{red} = 3.88$), to $\tau_1 = 15.2$ ns and $\tau_2 = 0.9$ ns (mean $\chi^2_{red} = 4.34$), $\tau_1 = 14.6$ ns and $\tau_2 = 0.7$ ns (mean $\chi^2_{red} = 2.9$), and $\tau_1 = 14.0$ ns and $\tau_2 = 1.3$ ns (mean $\chi^2_{red} = 4.1$), respectively (nonnormalized data $\chi^2_{red} \leq 20$).

Table 2. This table summarizes the fluorescence lifetime results from cell measurements in the presence and absence of amsacrine, the fluorophore quencher

	0 μM	18.6 μM	27.9 μM	37.2 μM
EB intensity percentage decrease	0%	2%	19%	24%
EB mean lifetime (tau1)	15.9 ns	15.2 ns	14.6 ns	14.0 ns
EB mean lifetime (tau2)	0.9 ns	0.9 ns	0.7 ns	1.3 ns
Mean reduced-Chi-square errors	3.88	4.34	2.9	4.1

The two-lifetime components determined are listed as the reduced mean χ^2 for the comparison between experiment and model. The average decrease in fluorescence intensity is also provided.

3.5 Fluorescence proteins expressed in living cells

Fluorescence lifetime measurements were obtained from viable CHO-K1 cells that exogenously express the fluorescent protein tdTomato. The Fig. 4D histogram provides a fluorescence lifetime distribution obtained from tdTomato expressing CHO-K1 cells using the FLECKD system. Based on our deconvolution analysis of single-exponential decay using values obtained from approximately 500 viable cells (gate 1), our results indicate that the tdTomato protein had an average fluorescence lifetime of 2.4 ns with a SD of 1.7 ns (mean

$\chi^2_{red} = 7.9$). This fluorescence lifetime value is consistent with previously published results [46]. In data not shown, we verified that the fluorescence and side scatter structural profile for CHO-K1 cells expressing and not expressing fluorescence proteins is identical; this confirms there were no light scatter changes present owing to possible morphology changes internal to the cell because of DNA transfection and fluorescent protein expression.

4 Concluding remarks

The development of a flow cytometer that can simultaneously measure multiple fluorescence decays has not been hitherto possible, mainly owing to the limitations of frequency-domain systems, as well as the single-pass nature of interrogation in flow cytometers. Here we demonstrate a new approach that will not only collect fluorescence intensity and scatter measurements, but also >1 fluorescence lifetime parameter. The FLECKD instrument is designed to reduce the excitation time to 25 ns, which was an adequate resolution for the fluorescence decay examples tested herein. Using a variety of fluorophores in both cells and microspheres, we demonstrate this approach can measure single- and double-exponential decays.

Certain factors can impact this approach and it is noteworthy to add that aggregates of two or more cells measured at once, imbalanced fluorescent labels across a given cell, rapid photobleaching for any given fluorophore, and large ratios of the sample diameter relative to the beam height can alter the waveform that is needed for fluorescence decay fitting. However algorithms and signal processing approaches performed on each dataset can mitigate these issues.

In general, the fluorescence lifetime as a parameter in cytometry can alleviate issues of spectral overlap with autofluorescence, dim fluorescence proteins (i.e. 1–5 ns lifetime species), and standard organic fluorophores (1–30 ns lifetime species) [47]. Additionally, more quantitative and intensity-independent measurements could be implemented for use with in vitro assays based on microfluidic, spectroscopic, and electrophoretic systems. This contribution adds to the growing popularity of time-resolved fluorescence measurement techniques and introduces a new approach to extracting fluorescence decay. The FLECKD system takes advantage of improvements in laser technology, digital signal processing, and data acquisition. Therefore as applications of fluorescence lifetime in flow cytometry continue to expand, kinetic dithering may play a large role in single-cell analysis and cell sorting.

The authors would like to thank Mark Naivar for his input and support on this project. The authors would also like to thank the Tsien Laboratory for donating the tdTomato DNA plasmid sample, and the NMSU NIH Minority Access to Research Careers (GM07668–36) for supporting Maryann Castillo. This work was supported by NSF CAREER award DBI-1150202.

The authors have declared the following potential conflict of interest: Dr. Giacomo Vacca is founder and owner of Kinetic River Corporation. All other authors declare no conflict of interest.

5 References

[1] Li, X., Lewis, M. T., Huang, J., Gutierrez, C., Osborne, C. K., *J. Natl. Cancer Inst.* 2008, *100*, 672–679.

[2] Shapiro, H. M., *Practical Flow Cytometry*, Wiley, Hoboken, NJ 2005.

[3] Perfetto, S. P., Chattopadhyay, P. K., Roederer, M., *Nat. Rev. Immunol.* 2004, *4*, 648–655.

[4] Houston, J. P., Naivar, M. A., Freyer, J. P., *Cytom. Part A.* 2010, *77*, 861–872.

[5] Steinkamp, J. A., Keij, J. F., *Rev. Sci. Instrum.* 1999, *70*, 4682–4688.

[6] Steinkamp, J. A., Yoshida, T. M., Martin, J. C., *Rev. Sci. Instrum.* 1993, *64*, 3440–3450.

[7] Pinsky, B. G., Ladasky, J. J., Lakowicz, J. R., Berndt, K., Hoffman, R. A., *Cytometry* 1993, *14*, 123–135.

[8] Houston, J. P., Naivar, M. A., Jenkins, P., Freyer, J. P., *Curr. Protocols Cytom.* 2012, *59*, 1.25.1–1.25.21.

[9] Rachofsky, E. L., Osman, R., Ross, J. B. A., *Biochemistry* 2001, *40*, 946–956.

[10] Pepperkok, R., Squire, A., Geley, S., Bastiaens, P. I. H., *Curr. Biol.* 1999, *9*, 269–272.

[11] McCormack, E., Micklem, D. R., Pindard, L.-E., Silden, E., Gallant, P., *Mol. Imag.* 2007, *6*, 193–204.

[12] Albertazzi, L., Arosio, D., Marchetti, L., Ricci, F., Beltram, F., *Photochem. Photobiol.* 2009, *85*, 287–297.

[13] Kneen, M., Farinas, J., Li, Y. X., Verkman, A. S., *Biophys. J.* 1998, *74*, 1591–1599.

[14] Gohar, A., Cao, R., Jenkins, P., Li, W., Houston, J. P., *Biomed. Opt. Express* 2013, *4*, 1390–1400.

[15] Bridgett, K. A., King, T. A., *Proc. Phys. Soc.* 1967, *92*, 75–78.

[16] Lewis, C., Ware, W. R., Doemeny, L. J., Nemzek, T. L., *Rev. Scient. Instrum.* 1973, *44*, 107–114.

[17] Loeser, C. N., Maher, M., Tarkmeel, H., Clark, E., *Exp. Cell Res.* 1972, *72*, 480–484.

[18] Koppel, D. E., Axelrod, D., Schlessinger, J., Elson, E. L., Webb, W. W., *Biophys. J.* 1976, *16*, 1315–1329.

[19] Arndt-Jovin, D. J., Latt, S. A., Striker, G., Jovin, T. M., *J. Histochem. Cytochem.* 1979, *27*, 87–95.

[20] Bottiroli, G., Prenna, G., Andreoni, A., Sacchi, C. A., Svelto, O., *Photochem. Photobiol.* 1979, *29*, 23–28.

[21] Docchio, F., Ramponi, R., Sacchi, C. A., Bottiroli, G., Freitas, I., *J. Microsc.* 1984, *134*, 151–160.

[22] Murray, J. G., Cundall, R. B., Morgan, C. G., Evans, G. B., Lewis, C., *J. Phys. E, Scient. Instrum.* 1986, *19* , 349–355.

[23] Yoshida, T. M., Barisas, B. G., *Biophys. J.* 1986, *50*, 41–53.

[24] Velez, M., Axelrod, D., *Biophys. J.* 1988, *53*, 575–591.

[25] Keating, S. M., Wensel, T. G., *Biophys. J.* 1991, *59*, 186–202.

[26] Martin-Fernandez, M. L., Tobin, M. J., Clarke, D. T., Gregory, C. M., Jones, G. R., *Rev. Scient. Instru.* 1998, *69*, 540–543.

[27] Verveer, P. J., Squire, A., Bastiaens, P. I. H., *Biophys. J.* 2000, *78*, 2127–2137.

[28] Gerritsen, H. C., Asselbergs, M. A. H., Agronskaia, A. V., Van Sark, W., *J. Microsc.* 2002, *206*, 218–224.

[29] Becker, W., Bergmann, A., Hink, M. A., Konig, K., Benndorf, K., *Microsc. Res. Techn.* 2004, *63*, 58–66.

[30] McLoskey, D., Campbell, D., Allison, A., Hungerford, G., *Meas. Sci. Technol.* 2011, *22*, 067001.

[31] Li, Z., Kawahito, S., Yasutomi, K., Kagawa, K., Ukon, J., *IEEE Trans. Electron. Dev.* 2012, *59*, 2715–2722.

[32] Pande, P., Applegate, B. E., Jo, J. A., *Biomed. Optic. Express* 2012, *3*, 2244–2262.

[33] Hotzer, B., Ivanov, R., Altmeier, S., Kappl, R., Jung, G., *J. Fluoresc.* 2011, *21*, 2143–2153.

[34] van Zandvoort, M. A., de Grauw, C. J., Gerritsen, H. C., Broers, J. L., oude Egbrink, M. G., Ramaekers, F. C., Slaaf, D. W., *Cytometry* 2002, *47*, 226–235.

[35] Lin, H. J., Herman, P., Lakowicz, J. R., *Cytomet. A J. Internat. Soc. Anal. Cytol.* 2003, *52*, 77–89.

[36] van Manen, H. J., Verkuijlen, P., Wittendorp, P., Subramaniam, V., van den Berg, T. K., Roos, D., Otto, C., *Biophys. J.* 2008, *94*, L67–L69.

[37] Hotzer, B., Ivanov, R., Brumbarova, T., Bauer, P., Jung, G., *FEBS J.* 2012, *279*, 410–419.

[38] Szmacinski, H., Lakowicz, J. R. *Cell Calc.* 1995, *18*, 64–75.

[39] Suhling, K., Davis, D. M., Phillips, D., *J. Fluoresc.* 2002, *12*, 91–95.

[40] Luce, R. D., *Response Times: Their Role in Inferring Elementary Mental Organization3*, Oxford University Press, New York, NY 1986.

[41] Davis, L. M., Harvey, J. D., Baguley, B. C., *Chemico-biological Interact.* 1987, *62*, 45–58.

[42] Datta, A., Mandal, D., Pal, S. K., Bhattacharyya, K., *J. Phys. Chem. B* 1997, *101*, 10221–10225.

[43] Hernández, L. I., Zhong, M., Courtney, S. H., Marky, L. A., Kallenbach, N. R., *Biochem.* 1994, *33*, 13140–13146.

[44] Jenkins, P. L., Freyer, J. P., Naivar, M. S., Arteaga, A., Houston, J. P., *Proc. SPIE7902* 2011, 790216–790218.

[45] Barton, J. K., Kumar, C. V., Turro, N. J., *J. Am. Chem. Soc.* 1986, *108*, 6391–6393.

[46] Pliss, A., Zhao, L., Ohulchanskyy, T. Y., Qu, J., Prasad, P. N., *ACS Chem. Biol.* 2012, *7*, 1385–1392.

[47] Lakowicz, J. R., *Principles of Fluorescence Spectroscopy*, Springer, New York, NY 2007.

